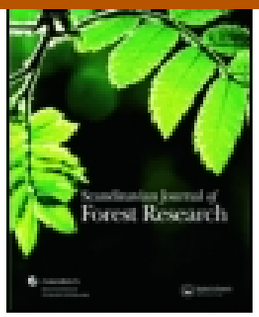

Scandinavian Journal of Forest Research

ISSN: 0282-7581 (Print) 1651-1891 (Online) Journal homepage: http://www.tandfonline.com/loi/sfor20

Effect of forest structure and health on the relative surface temperature captured by airborne thermal imagery -- – Case study in Norway Spruce-dominated stands in Southern Finland

Samuli Junttila, Mikko Vastaranta, Jarno Hämäläinen, Petri Latva-käyrä, Markus Holopainen, Rocío Hernández Clemente, Hannu Hyyppä & Rafael M. Navarro-Cerrillo

To cite this article: Samuli Junttila, Mikko Vastaranta, Jarno Hämäläinen, Petri Latva-käyrä, Markus Holopainen, Rocío Hernández Clemente, Hannu Hyyppä & Rafael M. Navarro-Cerrillo (2016): Effect of forest structure and health on the relative surface temperature captured by airborne thermal imagery -- – Case study in Norway Spruce-dominated stands in Southern Finland, Scandinavian Journal of Forest Research, DOI: 10.1080/02827581.2016.1207800

To link to this article: http://dx.doi.org/10.1080/02827581.2016.1207800

Accepted author version posted online: 04 Jul 2016.
Published online: 04 Jul 2016.

Publisher: Taylor & Francis & Informa UK Limited, trading as Taylor & Francis Group
Journal: *Scandinavian Journal of Forest Research*
DOI: 10.1080/02827581.2016.1207800

RESEARCH ARTICLE

Effect of forest structure and health on the relative surface temperature captured by airborne thermal imagery – Case study in Norway Spruce-dominated stands in Southern Finland

Samuli Junttila [a,b,*], Mikko Vastaranta [a,b], Jarno Hämäläinen [c], Petri Latva-käyrä [c], Markus Holopainen [a,b], Rocío Hernández Clemente [d], Hannu Hyyppä [b,e] and Rafael M. Navarro-Cerrillo [d]

[a] Department of Forest Sciences, University of Helsinki, Helsinki, Finland; Tel.: +358294158115 E-Mails: samuli.junttila@helsinki.fi (S.J.); mikko.vastaranta@helsinki.fi (M.V.); markus.holopainen@helsinki.fi (M.H.); [b] Centre of Excellence in Laser Scanning Research, Finnish Geospatial Research Institute FGI, FI-02431 Masala, Finland; Tel.: +358505122520 E-Mail: hannu.hyyppa@aalto.fi (H.H.) [c] Arbonaut Ltd., Kaislakatu 2, 80130, Joensuu, Finland; Tel.: +358132591911 E-Mails: jarno.hamalainen@arbonaut.com (J.H.); petri.latva-kayra@arbonaut.com (P.L-K.) [d] Department of Forestry Engineering, TreeSatLab, University of Cordoba. Edf. Leonardo da Vinci, Campus de Rabanales 14080 Cordoba, Spain.; Tel.: +34957218433 E-Mails: rociohc@uco.es (R.H.C.); rmnavarro@uco.es (R.N-C.) [e] Department of Built Environment, Aalto University, P.O.Box 15800, 00076 AALTO, Finland. Tel.: +358 50 560 3873

***** Author to whom correspondence should be addressed; E-Mail: samuli.junttila@helsinki.fi; Tel.: +358407153477.

Acknowledgments

We would like to thank Katri Tegel and Tuija Suihkonen from Arbonaut Ltd. for assisting with the field measurements.

Funding

The airborne scanning LiDAR, thermal and plot datasets applied in the paper have been made available by Arbonaut Ltd., within the scope of the THERMOLIDAR project. The THERMOLIDAR project is funded under the Framework 7 Theme Research for the benefit of SMEs under the Capacities Program of the European Commission. The Academy of Finland is acknowledged for its financial support, in the form of the Centre of Excellence in Laser Scanning Research (CoE-LaSR). This work was supported by The Finnish Society of Forest Science under Grant [number 201510040].

The effect of forest structure and health on the relative surface temperature captured by airborne thermal imagery was investigated in Norway Spruce-dominated stands in Southern Finland. Airborne thermal imagery, airborne scanning light detection and ranging (LiDAR) data and 92 field-measured sample plots were acquired at the area of interest. The surface temperature correlated most negatively with the logarithm of stem volume, Lorey's height and

the logarithm of basal area at a resolution of 254 m^2 (9-m radius). LiDAR-derived metrics: the standard deviations of the canopy heights, canopy height (upper percentiles and maximum height) and canopy cover percentage were most strongly negatively correlated with the surface temperature. Although forest structure has an effect on the detected surface temperature, higher temperatures were detected in severely defoliated canopies and the difference was statistically significant. We also found that the surface temperature differences between the segmented canopy and the entire plot were greater in the defoliated plots, indicating that thermal images may also provide some additional information for classifying forests health status. Based on our results, the effects of forest structure on the surface temperature captured by airborne thermal imagery should be taken into account when developing forest health mapping applications using thermal imagery.

Keywords: Remote sensing; defoliation; airborne thermal imagery; Ips typographus; forest mensuration and management; airborne laser scanning; forest health

Introduction

The world's climate has changed in the last decades due to human activities, causing a rise in global surface temperatures (Solomon et al. 2007). The rising temperatures are affecting insect pests' distribution and phenology, which, along with other climate-induced stress factors, has resulted in increased forest damage (Allen et al. 2010; Seidl et al. 2008). The rate of change in mean annual temperature is greater at higher latitudes than around the equator (Solomon et al. 2007); hence, the effects of climate change on insect species are stronger in boreal forests. Therefore, novel methods are required to accurately monitor and predict changes in the distribution of and damage from pest organisms.

The European spruce bark beetle (*Ips typographus*, L.) is a common species in Europe. The bark beetle requires fresh spruce timber to reproduce, but it can attack weakened living spruce trees or even healthy spruce trees when they appear in abundant numbers (Heliövaara et al. 1998). Bark beetle damage can be detected as discoloration and defoliation of the crown and as holes and resin flow traces on the bark. The European spruce bark beetle causes the largest economic losses to forest owners among insect pests in Eurasia (Wermelinger 2004). The last several decades have been marked by many storms, which have weakened and fallen vast amounts trees (Vastaranta et al. 2012). This has enabled reproduction of bark beetles resulting in large areas of damaged forest with high timber value. In Finland, Sweden and Norway, one generation of *I. typographus* is normally produced per year (Annila 1969; Bakke 1983). During the warm summers of 2010 and 2011, second generations of *I. typographus* were observed in southern Finland, causing more damage to forests (Neuvonen et al. 2014; Pouttu & Annila 2010). Increasing spring temperatures have affected the onset of the first *I. typographus* generation's development, supporting the development of a second generation (Faccoli 2009). One-third (30%) of the total stem volume of Finnish forests is comprised of Norway spruce (Korhonen et al. 2013); thus, it is important to develop methods to avoid and monitor probable bark beetle damages in the future.

The extent of forest damages varies from individual trees to several thousands of hectares; thus, the methods used to detect damages are different, depending on the scale and required level of detail (Vastaranta et al. 2012; Wulder et al. 2006). The intensity of forest management also varies between countries, and thus so too do the objectives of mapping forest damages. In countries where extensive forest management is applied, thousands of hectares of forest may be damaged and the only operational method of mapping is the use of remote sensing. Satellite-based (e.g. MODIS, Landsat) remote-sensing methods are widely used in these countries (Coops et al. 2006; Coops et al. 2009a; Coops et al. 2009b; Eklundh et al. 2009; Luther et al. 1997; Radeloff et al. 1999; Townsend et al. 2012; White et al. 2005; Wulder et al. 2008), although the output accuracy may only be suitable for large-scale mapping. In Finland and other countries where intensive forest management is practiced, detailed mapping of the damages is required. For example, even a small group of damaged trees has to be removed from the forest by the forest owner due to legislation and forest owners can receive compensation from insurance companies if the amount of damaged wood is over 10 m^3/ha.

For a detailed mapping of defoliation (i.e., tree or sample plots), possibilities involving both active and passive airborne sensors have been investigated. Airborne scanning light detection and ranging (LiDAR)–based methods can capture vegetation heights and thus may have some potential because LiDAR pulses seem to penetrate defoliated canopies more than they do healthy canopies (Kantola et al. 2013; Kantola et al. 2010; Solberg et al. 2006; Vastaranta et al. 2013a). However, these methods have many uncertainties, since the canopy density is also affected by factors other than defoliation. Lausch et al. (2013) studied hyperspectral remote-sensing techniques to predict the potential for bark beetle outbreaks based on the mapped spruce forest's vitality at different scales. The hyperspectral remote-sensing data used had 4-m and 7-m ground resolutions. Based on the study, they were able to recognize three different vitality classes of spruce forest from the hyperspectral data, indicating the different stages of *Ips typographus* attack. However, the accuracy of the predicted observed effects was 69%, which can be considered insufficient for many forestry practices. Fassnacht et al. (2014) were able to develop a method using hyperspectral imagery with 5-m and 7-m ground resolutions for mapping bark beetle-induced tree mortality. The mapping of dead trees was possible with notably higher overall accuracies (84%–96%). The detection of dead and defoliated spruces was studied using aerial photography at the single-tree level (Haara & Nevalainen 2002). When using a three-class classification scheme for the defoliation, 89.5% of the plots were classified correctly. Kantola et al. (2010) investigated the combination of airborne scanning LiDAR and aerial photography in classifying the defoliation of pines at the single tree-level. They showed that the inclusion of aerial photography improved the accuracy of defoliation classification.

As far as we know, the effect of forest structure on airborne thermal imagery has not been studied intensively. Sader (1986) studied the effective radiant temperatures in a mountainous Pacific Northwest forest at stand-level using thermal infrared multispectral scanner (TIMS) data at 10 m resolution. He found that old growth forest stands (undisturbed forest) with greater amounts of biomass and closed canopies had temperatures that were 2.5°C and 8–9°C lower than younger, less dense stands aged 25–33 and 0–12 years, respectively. Sader (1986) also found that the aspect and slope gradient had greater effects on thermal emission in younger reforested clearcuts than in older stands, where the effects were minor. Peterson et al. (1986) analysed forest structures at plot-level (0.1 ha) using the Daedalus Airborne Thematic Mapper (ATM) data at 23-m resolution and found long-wave thermal radiation to be negatively correlated with basal area and canopy closure. Scherrer et al. (2011) studied the drought-sensitivity of several deciduous tree species based on high-resolution (20 cm resolution) thermal imagery. They found that canopy architecture had an influence on canopy temperature, dense canopies being warmer than open canopies in the warm summer climate in Switzerland.

Thermal imagery measures thermal emissions from surfaces and could be a useful method for forest health and defoliation mapping. As a tree loses its needles, its evaporative surface area decreases and canopy and leaf architecture changes causing microclimatic conditions to transform as air space increases inside the tree crown. This causes changes in the temperature of the tree canopy, which can be detected through thermal imaging (Dennison et al. 2009; Scherrer et al. 2011). Higher canopy temperatures were found in pine trees under moisture stress and bark beetle attack than in healthy trees in the same area (Olson 1972; Weber 1971). Stressed trees were as much as 6 °C warmer than the control trees but the average temperature differences between the stressed and the healthy control trees were minor—only 1 °C; they were also unable to determine if the differences were due to physiological stress or variation in the microclimate (Olson 1972; Weber 1971).

More recent studies investigating the use of thermal imagery in plant health monitoring suggests the potential of thermal imaging in operational plant management (Bulanon et al. 2008; Grant et al. 2006; Grant et al. 2007; Zarco-Tejada et al. 2012). A rise in the surface temperature of defoliated tree crowns can be visible due to the reduction of leaf stomatal conductance or defoliation (Calderón et al. 2013; Clark et al. 2012; Dennison et al. 2009; Hernández-Clemente et al. 2011). Canopy structure also affects surface temperature acquired with thermal infrared imaging (Scherrer et al. 2011); thus, there may be a possibility of mapping defoliation on a thermal basis in boreal spruce forests.

Here, the effect of forest structure and health status of a Norway spruce (*Picea abies* L.) forest on high-resolution (1 m x 1 m) thermal imagery was studied using 9-m radius field plots in southern Finland. The forest health status in the study area varied due to a bark beetle (*Ips typographus* L.) infestation, causing defoliation of the trees. The hypothesis was that defoliated stands could be distinguished as warmer plots than healthy plots using airborne thermal imagery. Although defoliated trees and canopies could be detected as warmer, presumably many uncertainties also exist due to the possible effect of the forest structure on the recorded temperatures. Thus, we also aimed to investigate the effect of forest structure on the detected temperature.

Material and methods

Study area

The study site is located in the Askola municipality in Southern Finland (60°31′59″ N, 25°36′00″ E, Figure 1). The location was selected, with assistance from the Finnish Forest Center, due to existing defoliation damages caused by *I. typographus* during the last several years. The area of the study site is 3,450 hectares in total, comprising 2,340 hectares of forest and 1,110 hectares of agricultural and built land. Norway spruce (*Picea abies*, L.) mainly dominates forests in this area, with mixtures of silver birch (*Betula pendula*, Roth), downy birch (*Betula pubescens*, Ehrh.), Scots pine (*Pinus sylvestris*, L.) and, to a lesser degree, rowan (*Sorbus aucuparia*, L.), aspen (*Populus tremula*, L.) and common juniper (*Juniperus communis*, L.). Scots pine-dominated forests are less common in the study area. The forest types represented here mainly range from heath with rich grass-herb vegetation to heath with blueberry-dominated vegetation. These types are from OMT to MT on Cajander's classification, and are quite eutrophic to Finnish forests (Cajander 1926).

An additional 39 plots were obtained from the Finnish Forest Center (FFC) and were added to the analyses, in order to obtain more information from healthy forests. These plots were measured in 2011 in a similar manner and included respective forest inventory attributes, but without information on the forest health.

Aerial imagery provided by the National Land Survey (NLS) from 2013 was used to visually evaluate if the FFC plots were healthy and did not have defoliated trees. Eye calibration was done with the defoliation data measured in the fall of 2013, enabling a coarse visual classification of damages or no damages. Three plots were visually classified as damaged and were not included (n = 3) in the data analysis due to missing data on the amount of defoliated stem volume, as the healthy plots were used in the forest structure analysis.

It should be noted that there was a two-year gap between the two ground plot datasets; the effect of the gap was therefore examined by re-measuring 11 plots that were measured in 2011. The average growth after two years was 0.5 cm in *Dg* and 0.2 m in *Hg* at plot-level. Thus, the effect of growth was considered to be marginal in our analyses, and the plots from 2011 and 2013 were merged.

Thermal data

The thermal imaging data were acquired from an airplane on 25th of September in 2013 between 16:40 and 18:15 local time (GMT+2). The thermal survey camera used was an Optech CM-LW640 (Optech International Inc., Kiln, Mississippi, USA), with a 35 mm lens delivering images at 1-meter spatial resolution from 2,000 meters above ground. It is based on an uncooled microbolometer sensor with a resolution of 640 x 480 pixels. The camera is designed to perceive thermal emissions at the longer thermal infrared wavelength area of 8–14 μm and is geometrically calibrated. Temperature stabilization is ensured with integrated parameterized nonuniformity corrections (NUC) and an athermal lens design. The flying altitude was 2,000 meters above sea level. The sensor did not have a self-calibration procedure. Weather conditions affect surface temperature; therefore, weather data were collected from a road weather station operated by the Finnish Meteorological Institute (FMI), ~10 km from the research area. The average temperature at the time of the thermal data acquisition was 2.5 C°, with a relative humidity of 89%. Some drizzle occurred before the data collection and the wind speed was around 2–3 meters/second. Transpiration rate at this temperature and humidity is near to zero.

The thermal survey camera only recorded relative temperatures on one 8-bit channel, with values ranging from 0 to 255. In-situ temperature measurements were not performed; thus, the relative values cannot be transformed into absolute temperature values. The individual images were normalized by the data provider (Fugro Survey Ltd.) using an in-house calibration method based on image overlap to create a thermal image mosaic for the whole study area at 1-m resolution. Geolocation accuracy of the thermal imagery was 1-meter (1 pixel).

LiDAR data

The LiDAR data were collected at the same time as the thermal data. The system was set to record multiple echoes. The LiDAR returns included the coordinates (x, y), height values (z), intensity values (from 1 to 180), flight line numbers and echo types. The echoes were classified into four classes: 1 = only echo, 2 = first echo, 3 = intermediate echo and 4 = last echo. The scanner used was an Optech LW640. The field of view was 13 degrees, the pulse rate was 50 kHz, the scanning frequency was 42 Hz and the beam divergence was 0.25 mrad. The average pulse density of the resulting data was 1.8 pulses / m².

The LiDAR data were classified into ground and non-ground points using the standard TerraScan approach, where a filtering algorithm based on triangular irregular networks (TIN) is applied (Axelsson 2000). A digital elevation model (DEM) was created using classified ground points for the study area. A canopy height model (CHM) was created using the highest laser points for the whole study area at a 1-m resolution.

Field measurements

The field measurements were carried out during October and November in 2013. A total of 53 plots (Table 1) with 9-m radius (~254 m^2) were established in Norway spruce-dominated forest stands. The sampling of the plots was based on following steps:

(1) The forest attribute maps provided by the Finnish National Forest Inventory were used to locate Norway spruce-dominated stands (Korhonen et al. 2013). The structural criteria for plot selection were spruce dominance (over 70% of total volume) and age (over 30 years old).
(2) Prior to going to the field, the plots were positioned approximately, according to the thermal imagery, to maximize the variability of the thermal image data.
(3) Clusters of three plots were formed so that local variability of the thermal imagery would be maximized; local maximum, minimum and mean temperature values were represented.

Then, the plots were positioned with a Trimble Pro XH (Trimble Navigation Ltd., Sunnyvale, California, USA), which can reach an accuracy of 30 cm. Differential correction of the plot centers was applied with the GPS Pathfinder Office software (Trimble Navigation Ltd., Sunnyvale, California, USA).

The forest inventory attributes were measured from the sample plots. The basal-area (*G*) and basal-area weighted mean diameter (*Dg*) was calculated from the diameter at breast height (dbh) measurements of all trees with dbh > 5 cm. Calipers were used to measure dbh. The heights of the species-specific basal-area median trees were measured using a Vertex tree height–measuring device. Then, the heights of all trees were calculated using Veltheim's height models (Veltheim 1987). The mean heights (*Hg*) of the trees within the sample plots were calculated as the basal area–weighted mean height, or the so-called Lorey's height. The stem volume (*Vol*) was calculated as the sum of the tree-wise stem volumes, computed with allometric stem volume functions (Laasasenaho 1982). The stand age was computed using functions based on site index from Vähäsaari (1988).

The health status of each tree was visually assessed. Three classes were used: defoliation, discoloration and the presence of bark beetles, in addition to classifying the trees as dead or alive. Each of these had two classes: present or not present. Defoliation and discoloration were marked as present when they were noticeable to the naked eye. The threshold level of defoliation was 20% (compared to a healthy tree within the same site type), which is considered to be visually noticeable

(Eichhorn et al. 2004).

The percentage of stem volume of defoliated trees (*Defol_V*) in a sample plot was computed by summing the stem volumes of the damaged trees and dividing it by sample plot's total stem volume. The percentage of stem volume of dead trees (*Dead_V*) was computed respectively.

An additional 39 plots were obtained from the Finnish Forest Center (FFC) and were added to the analyses, in order to obtain more information from healthy forests. These plots were measured in 2011 in a similar manner and included respective forest inventory attributes, but without the information on forest health.

Aerial imagery provided by the National Land Survey (NLS) from 2013 was used to visually evaluate if the FFC plots were healthy and did not have defoliated trees. Calibration of visual interpretation was done with the defoliation data measured in the fall of 2013, enabling a coarse visual classification of damaged and undamaged sample plots. Three plots were visually classified as damaged and were not included (n = 3) in the data analysis due to missing data on the amount of defoliated stem volume, as the healthy plots were used in the forest structure analysis.

It should be noted that there was a two-year gap between the two ground plot datasets; the effect of the gap was therefore examined by re-measuring 11 plots that were measured in 2011. The average growth after two years was 0.5 cm in *Dg* and 0.2 m in *Hg* at plot-level. Thus, the effect of growth was considered to be marginal in our analyses, and the plots from 2011 and 2013 were merged.

Data processing

Thermal data

Statistical features from the thermal data were calculated for the plots (Table 2). Two different approaches were applied: 1) First, mean temperatures and their standard deviations were calculated at 256-m^2 resolution; 2) second, a forest mask was created from the CHM, and thermal metrics were calculated for responses above 3 m without the ground or the understory vegetation. By using this approach, it was possible to estimate the relative surface temperature of the tree crowns for the plots. The ground surface temperature was estimated using the same method, but only responses below three meters were included.

The $plot_{mean}$, $canopy\text{-}only_{mean}$ and $ground\text{-}only_{mean}$ values represent the arithmetic mean of the relative surface temperature values calculated for the entire plot, the segmented canopy and the ground, respectively. The min values represent the minimum temperature value measured from the plot or the canopy. The max values represent the maximum temperature value measured from the plot or the canopy.

LiDAR

A suite of 30 LiDAR features (Table 3) describing canopy height and density was extracted using the ArboLiDAR software package (Arbonaut Oy, Joensuu, Finland) according to Junttila et al. (2010). The LiDAR metrics were designed to predict forest stand characteristics, such as mean height, stem number and stem volume (Junttila et al. 2010; Naesset 1997; Næsset & Bjerknes 2001). The most suitable LiDAR features were selected from the suite according to preliminary analysis. In addition, slope, aspect and forest canopy cover percentage were calculated from the LiDAR data.

Statistical analyses

Effect of forest structure on relative surface temperature

The effect of forest structure on relative surface temperature was studied using only the healthy plots (n = 43) that had less than 3% of *Defol_V* and less than 6% of *Dead_V* . Linear regression analyses were used to explore the empirical relationships between the thermal features as our response, along with forest structural variables (*Vol*, *Age*, *Hg*, *Dg*, *G* and stem number) as the predictors. The analyses were performed for both in-situ measured forest structural variables and the LiDAR variables (*i.e.*,

CHM, H90 and CHM_std).

Effect of forest structure and health on relative surface temperature

The sample plots measured in fall 2013 with information on defoliation were used to analyse dependencies between surface temperature, forest structure and forest health. The plot data was supplemented with 10 randomly selected healthy plots from the FFC data to obtain an even distribution of the defoliated and healthy plots. The total number of plots in these analyses was 63.

Then, healthy and defoliated plots were compared in four groups by stem volume (Table 4). A plot was counted as "healthy" if it had less than 3% of *Defol_V* and as "defoliated" if it had over 10% of *Defol_V*. The relative mean surface temperatures of the plots within groups were then compared with t-tests. The differences between the thermal responses from the canopy and the ground were also examined.

Groups with different amounts of *Defol_V* were formed, using only plots with over 100 m^3/ha of stem volume to partially hinder the effect of forest structure . Healthy plots (n = 11) were determined using the same limit of *Defol_V* as before (3%). The "Defoliated 10%" group (n = 12) had 10–20% of *Defol_V*, while the "Defoliated 20%" group (n = 11) had over 20% of *Defol_V*.

Finally, multiple regression analysis was used to examine the dependencies between surface temperature, forest structure and forest health. Forest structural variables including airborne scanning LiDAR features were entered into the multiple regression analysis with *Defol_V* one at a time as explanatory variables, in addition to surface temperature as a dependent variable.

Results

The effect of forest structure on relative surface temperature

A negative linear relationship was found between canopy height and relative surface temperature (r = –0.72) (Figure 2), *i.e.*, mature trees are colder than young, short ones. The *Hg* had a respective linear relationship, with a correlation of –0.67. The logarithmic transformation of number of stems were also correlated with the temperature (r = 0.49). The logarithmic transformations of basal area and stem volume were correlated with surface temperature, with correlations of –0.75 and –0.78, respectively. Tree age was correlated with the surface temperature with a correlation of –0.58.

In addition to the field-measured forest structural variables, LiDAR-derived metrics describing canopy characteristics were used in the investigations (Figure 3). Height features such as CHM_mean, CHM_max and H90 were negatively correlated with the relative mean temperature, with correlations of –0.71, –0.73 and –0.73, respectively. This is consistent with the mean height measured in-situ. The standard deviation of CHM explained the variation in the relative mean temperature, with a correlation of –0.77. CHM_std was highly correlated with the CHM_max feature (r = 0.91); however, the standard deviation takes gaps in the canopy into account, which could explain the better correlation. Forest canopy cover percentage (FCC), as calculated from CHM, was nearly equal in explaining the variation in the relative mean temperature (r = –0.72). As forest cover percentage increased, the relative surface temperature decreased. CV, calculated as CHM_mean divided by CHM_std, was also correlated with the relative surface temperature (r = 0.65). CV decreased as height increased, and temperature increased as CV increased.

The effect of defoliation on relative surface temperature

The defoliated plots showed higher surface temperatures in all volume classes (Figure 4a). The defoliation damage was more severe in larger stem volume classes; the surface temperature differences between healthy and defoliated plots were also greater in these classes. However, the surface temperature varied inside the classes, especially in the volume classes with over 320 m^3/ha, which could partially hide the effect of defoliation on relative temperature.

The relative mean surface temperature was higher in the defoliated plots (Figure 4b). The plots with

over 20% of *Defol_V* (*Defoliated 20%*) had significantly (p = 0.04) higher surface temperatures than the healthy plots. The surface temperatures of the less defoliated plots (*Defoliated 10%*) had a larger interquartile range compared to the healthy and severely defoliated plots. Thus, although the mean surface value was higher than in the healthy plots, the difference was not statistically significant using Student's t-test (p = 0.05).

The temperature differences between the segmented canopy and the entire plot were greater by one relative temperature unit on average in the defoliated plots than in the healthy plots; however, the differences between the groups were not statistically significant (p = 0.07) (Figure 5a). The canopy seemed to be warmer where defoliation occurred, but deviation in surface temperature inside the groups diminished the differences, which could be caused by differences in the structure of the forest.

The surface temperature seemed to vary more in the defoliated plots than in the healthy plots. The standard deviations calculated for the entire plots seemed to increase in plots with over 10% defoliated tree volume (Figure 5b). However, no significant differences were found between the groups (p = 0.16).

Dependencies between surface temperature, forest structure and forest health In the data, logarithmic transformation of stem volume had the strongest correlation with the surface temperature (r = –0.78) and was further used as a variable in the multiple regression analysis, together with *Defol_V* to investigate dependencies between surface temperature, forest structure and amount of defoliation. The results showed that the amount of *Defol_V* had a statistically significant effect on the surface temperature (Table 5). As the *Defol_V* increased, the relative surface temperature increased as well, according to the regression analysis (Table 6). Increase in stem volume resulted in a decrease in the relative surface temperature. According to the analysis, the structural effect on relative surface temperature dominated over the effect of defoliation, as the p-value was lower for the logarithmic transformation of stem volume (p < 0.001).

Among the LiDAR features, the standard deviation in CHM had the strongest correlation with the mean relative temperature. Thus, it was also tested in the multiple regression analysis, together with the defoliated stem volume, to investigate their effects on the measured surface temperature. The estimates of *Defol_V* coefficients were similar between the analyses. It seemed that the relative mean temperature increased as the ratio of defoliated volume increased (Table 7). The structural effect on the relative surface temperature seemed to dominate over the effect of defoliation.

Discussion

In this study, the applicability of thermal imagery in mapping and monitoring forest structure and health status was investigated. Based on the analyses, it seems that the relative surface temperature decreases as the forest matures, i.e., stem volume, height, age, canopy closure and basal area increase. This is also supported by Peterson et al. (1986) and Sader (1986). Peterson et al. (1986) studied the effect of forest structure on thermal data from the Thematic Mapper Simulator (TMS) in the Sierra Nevadas, where canopy closure was negatively correlated with the thermal data (r = –0.65) and basal area (r = –0.31). Sader (1986) showed that younger age classes were contributing most of the variability in surface temperature related to terrain and that older stands had lower surface temperatures. This is consistent with our study, as the change in temperature was highest in young stands with low volume and decreased with age.

The sample plot data mainly included spruce-dominated forest, with some mixture of pine and birch. There was not enough data to analyse the effect of tree species on the surface temperature, which has been studied with broad-leaved trees by Scherrer et al. (2011). The canopy structure varies between the main tree species in Finland. Spruce canopies are denser than those of other species, which could affect the surface temperatures of tree canopies. Thus, more research is needed on the effect of tree species on thermal imagery in boreal forests.

Regarding the health status, our main finding was that the effects of forest structure on the surface

temperature hinder the mapping of defoliation; however, severely defoliated plots may be possible to map using thermal imagery. When the main aim is to map defoliation, the effect of the forest structure has to be taken into account. In this study, forest structural variables were measured in the field. In an operational application, detailed plot data are not usually available. However, many forest structural variables are highly correlated with LiDAR data (Vastaranta et al. 2013b) and can be used to normalize the effect of the forest structure. In our study, similar correlation coefficients were detected between the LiDAR features and surface temperature as with the forest structural variables. The strongest negative correlation was found between the standard deviations of CHM within the sample plots and mean surface temperatures. Height features, such as H90, CHM_max and CHM_mean, were also strongly correlated with surface temperature. Forest structural variables and LiDAR features were equal in explaining the surface temperature.

Higher surface temperatures were detected in the defoliated plots than the healthy plots in the thermal data. The mean surface temperatures were examined in four volume classes (to roughly normalize the effect of the forest structure), and the general trend was that the defoliated plots had a greater mean surface temperature than the healthy plots. The mean surface temperature was also examined in groups by defoliated stem volume. Severely defoliated plots showed significantly higher surface temperatures than the healthy plots (p = 0.04), although the mean temperature of the healthy and defoliated groups overlapped. The mean surface temperatures of the moderately defoliated plots were more dispersed, indicating that moderately defoliated plots may be difficult to distinguish from healthy plots with thermal imagery alone. The difference between the canopy mean and the entire plot mean surface temperature was greater in the defoliated than the healthy plots, but not statistically significant (p = 0.15). The difference increased as defoliation increased.

Boreal forest landscapes in Finland are heterogeneous in structure, and many factors affect the thermal radiation measured by thermal infrared cameras and scanners. Boreal forests are moist, and many peat lands have been drained for forest management, in order to improve forest growth. Wetness and moisture in forest canopies and soil affect the surface temperature and upcoming thermal radiation, as ditches could be distinguished from the thermal imagery as cold spots. Mira et al. (2009) found that the thermal emissivity of soil is strongly correlated with the soil moisture content, thus affecting the recorded surface temperature. Surface temperature has also been used in studies of soil moisture and water stress among plants (Alchanatis et al. 2010; Soliman et al. 2013).

Factors causing the differences in the surface temperature could derive from the weather condition which was cold and humid (relative humidity ~ 80–90%). Air temperature during the thermal imagery acquisition was low (~ 3 °C) , hence stomata is nearly closed and transpiration rate close to zero (Hällgren et al. 1982; Schwarz et al. 1997). Thus; it can be assumed that the differences in the surface temperature are not caused by changes in the transpiration rate. Surface water was seen as cold spots on the thermal imagery so it can be assumed that moisture on needles decreased their surface temperature. Defoliated canopies have less foliage and thus less leaf surface area for moisture to adhere. This could result in defoliated canopies having a higher surface temperature than healthy canopies. No in-situ moisture measurements were conducted; therefore we cannot validate this theory.

Initially the thermal imagery data acquisition was intended to take place in warmer weather conditions (13-20 °C), but practical issues with the data provider and unusually cold weather lead to delays resulting in the discussed weather conditions on the data acquisition date. However, the results of this study are promising considering future investigations in warmer temperatures as changes were detectable despite the cold weather during the data acquisition. The optimal timing for thermal imagery acquisition has not been studied in boreal forests and climate. More research is needed on the effect of the timing of thermal imagery acquisition and the effect of soil moisture on thermal imagery in boreal forests for optimal usage of the data.

A two-class classification scheme was used for defoliation in the ground plot measurements (defoliated or not), in which totally defoliated trees (~80–90% needle-loss) and slightly defoliated trees (~10–20% needle-loss) could both be assigned to the same class. This could have affected the

results, as it is not possible to separate the plots that have suffered more severe needle loss from the only slightly defoliated plots. Classification of healthy and defoliated forest stands cannot be done based solely on thermal imagery, as the surface temperature values of the healthy and the defoliated plots overlapped; however, monitoring of surface temperatures could possibly assist in locating stressed or defoliated areas.

In conclusion it was found that forest structure affects the relative surface temperature in addition to defoliation. In our study, the detected surface temperatures were partly overlapping between healthy and defoliated plots in moist and below 5 °C weather conditions, which hindered the detection of defoliation. More research is needed on the effect of weather conditions on thermal imagery for further analyses on the applicability of the studied methods for detecting defoliated forest areas. Forest canopy structure, as measured by scanning LiDAR, can be used to normalize structural effects, since the LiDAR features showed similar correlation with surface temperature as the field measured forest structural attributes.

Acknowledgments

We would like to thank Katri Tegel and Tuija Suihkonen from Arbonaut Ltd. for assisting with the field measurements.

Disclosure statement

The authors declare no conflict of interest.

Funding

The LiDAR, thermal and plot datasets applied in the paper have been made available by Arbonaut Ltd., within the scope of the THERMOLIDAR project. The THERMOLIDAR project is funded under the Framework 7 Theme Research for the benefit of SMEs under the Capacities Program of the European Commission. The Academy of Finland is acknowledged for its financial support, in the form of the Centre of Excellence in Laser Scanning Research (CoE-LaSR). This work was supported by The Finnish Society of Forest Science under Grant [number 201510040].

References and Notes

Alchanatis V, Cohen Y, Cohen S, Moller M, Sprinstin M, Meron M, Tsipris J, Saranga Y, Sela E. 2010. Evaluation of different approaches for estimating and mapping crop water status in cotton with thermal imaging. Prec Agric. 11: 27-41.
Allen CD, Macalady AK, Chenchouni H, Bachelet D, McDowell N, Vennetier M, Kitzberger T, Rigling A, Breshears DD, Hogg E. 2010. A global overview of drought and heat-induced tree mortality reveals emerging climate change risks for forests. For Ecol Manage. 259: 660-684.
Annila E. 1969. Influence of temperature upon the development and voltinism of *Ips typographus*, (L.) (Coleoptera, Scolytidae). Ann Zool Fenn. 6: 161–208.
Axelsson P. 2000. DEM generation from laser scanner data using adaptive TIN models. Int Arch Photogram Rem Sens. 33: 111-118.
Bakke A. 1983. Host tree and bark beetle interaction during a mass outbreak of *Ips typographus* in Norway. Zeits Angew Entom. 96: 118-125.
Bulanon D, Burks T, Alchanatis V. 2008. Study on temporal variation in citrus canopy using thermal imaging for citrus fruit detection. Biosys Eng. 101: 161-171.
Cajander AK. 1926. Theory of forest types.
Calderón R, Navas-Cortés JA, Lucena C, Zarco-Tejada PJ. 2013. High-resolution airborne hyperspectral and thermal imagery for early detection of *Verticillium* wilt of olive using fluorescence, temperature and narrow-band spectral indices. Remote Sens Environ. 139: 231-245.

Clark KL, Skowronski N, Gallagher M, Renninger H, Schäfer K. 2012. Effects of invasive insects and fire on forest energy exchange and evapotranspiration in the New Jersey pinelands. Agric For Meteorol. 166: 50-61.
Coops NC, Johnson M, Wulder MA, White JC. 2006. Assessment of QuickBird high spatial resolution imagery to detect red attack damage due to mountain pine beetle infestation. Remote Sens Environ. 103: 67-80.
Coops NC, Waring RH, Wulder MA, White JC. 2009a. Prediction and assessment of bark beetle-induced mortality of lodgepole pine using estimates of stand vigor derived from remotely sensed data. Remote Sens Environ. 113: 1058-1066.
Coops NC, Wulder MA, Iwanicka D. 2009b. Large area monitoring with a MODIS-based Disturbance Index (DI) sensitive to annual and seasonal variations. Remote Sens Environ. 113: 1250-1261.
Dennison PE, Nagler PL, Hultine KR, Glenn EP, Ehleringer JR. 2009. Remote monitoring of tamarisk defoliation and evapotranspiration following saltcedar leaf beetle attack. Remote Sens Environ. 113: 1462-1472.
Eichhorn J, Szepesi A, Ferretti M, Durrant D, Roskams P. 2004. Manual on methods and criteria for harmonized sampling, assessment, monitoring and analysis of the effects of air pollution on forests. Part II visual assessment of crown condition. International co-operative programme on assessment and monitoring of air pollution effects on forests. United Nations Economic Commission for Europe Convention on Long-Range Transboundary Air Pollution.
Eklundh L, Johansson T, Solberg S. 2009. Mapping insect defoliation in Scots pine with MODIS time-series data. Remote Sens Environ. 113: 1566-1573.
Faccoli M. 2009. Effect of weather on Ips typographus (Coleoptera Curculionidae) phenology, voltinism, and associated spruce mortality in the southeastern Alps. Environ Entomol. 38: 307-316.
Fassnacht FE, Latifi H, Ghosh A, Joshi PK, Koch B. 2014. Assessing the potential of hyperspectral imagery to map bark beetle-induced tree mortality. Remote Sens Environ. 140: 533-548.
Grant OM, Chaves MM, Jones HG. 2006. Optimizing thermal imaging as a technique for detecting stomatal closure induced by drought stress under greenhouse conditions. Physiol Plant. 127: 507-518.
Grant OM, Tronina Ł, Jones HG, Chaves MM. 2007. Exploring thermal imaging variables for the detection of stress responses in grapevine under different irrigation regimes. J Exp Bot. 58: 815-825.
Haara A, Nevalainen S. 2002. Detection of dead or defoliated spruces using digital aerial data. For Ecol Manage. 160: 97-107.
Heliövaara K, Peltonen M, Mannerkoski I, Siitonen J. 1998. [Finlands bark beetles (Coleoptera: Scolytidae)]. Helsinki (Finland): University of Helsinki, DoA Zoology. Finnish.
Hernández-Clemente R, Navarro-Cerrillo RM, Suárez L, Morales F, Zarco-Tejada PJ. 2011. Assessing structural effects on PRI for stress detection in conifer forests. Remote Sens Environ. 115: 2360-2375.
Hällgren JE, Sundbom E, Strand M. 1982. Photosynthetic responses to low temperature in Betula pubescens and Betula tortuosa. Physiol Plant. 54: 275-282.
Junttila V, Kauranne T, Leppänen V. 2010. Estimation of forest stand parameters from airborne laser scanning using calibrated plot databases. For Sci. 56: 257-270.
Kantola T, Vastaranta M, Lyytikäinen-Saarenmaa P, Holopainen M, Kankare V, Talvitie M, Hyyppä J. 2013. Classification of needle loss of individual Scots pine trees by means of airborne laser scanning. Forests. 4: 386-403.
Kantola T, Vastaranta M, Yu X, Lyytikainen-Saarenmaa P, Holopainen M, Talvitie M, Kaasalainen S, Solberg S, Hyyppa J. 2010. Classification of defoliated trees using tree-level airborne laser scanning data combined with aerial images. Remote Sens. 2: 2665-2679.
Korhonen KT, Ihalainen A, Viiri H, Heikkinen J, Henttonen HM, Hotanen J-P, Mäkelä H, Nevalainen S, Pitkänen J. 2013. [Finnish forests 2004-2008 and their development 1921-2008]. Metsätiet aikakausk. 3: 269–608. Finnish.
Laasasenaho J. 1982. Taper curve and volume functions for pine, spruce and birch [*Pinus sylvestris, Picea abies, Betula pendula, Betula pubescens*]. Commun Insti Fores Fenn. 108.
Lausch A, Heurich M, Gordalla D, Dobner H-J, Gwillym-Margianto S, Salbach C. 2013. Forecasting potential bark beetle outbreaks based on spruce forest vitality using hyperspectral remote-sensing techniques at different scales. For Ecol Manage. 308: 76-89.

Luther JE, Franklin SE, Hudak J, Meades JP. 1997. Forecasting the susceptibility and vulnerability of balsam fir stands to insect defoliation with Landsat Thematic Mapper data. Remote Sens Environ. 59: 77-91.
Mira M, Caselles V, Valor E, Coll C. 2009. Accurate assessment of land surface thermal emissivity. EARSeL eProceed. 8: 187-193.
Naesset E. 1997. Estimating timber volume of forest stands using airborne laser scanner data. Remote Sens Environ. 61: 246-253.
Næsset E, Bjerknes K-O. 2001. Estimating tree heights and number of stems in young forest stands using airborne laser scanner data. Remote Sens Environ. 78: 328-340.
[MetINFO - Forest health: european spruce bark beetle (*Ips typographus*) [Internet]. c2003-2014. Vantaa: Forest Research Institute; [cited 20.8.2014]. Available from: http://www.metla.fi/metinfo/metsienterveys/lajit_kansi/iptypo-n.htm. Finnish.
Olson CE. 1972. Remote sensing of changes in morphology and physiology of trees under stress. Houston, Texas: School of National Resources, University of Michigan,
Peterson DL, Westman WE, Stephenson NJ, Ambrosia V, Brass J, Spanner M. 1986. Analysis of forest structure using Thematic Mapper simulator data. IEEE Trans Geosci Remote Sens. 113-121.
Pouttu A, Annila E. 2010. [Two generations of european spruce bark beetle during summer 2010]. Metsätiet aikakausk. 4. Finnish.
Radeloff VC, Mladenoff DJ, Boyce MS. 1999. Detecting jack pine budworm defoliation using spectral mixture analysis: separating effects from determinants. Remote Sens Environ. 69: 156-169.
Sader SA. 1986. Analysis of effective radiant temperatures in a Pacific Northwest forest using thermal infrared multispectral scanner data. Remote Sens Environ. 19: 105-115.
Scherrer D, Bader MK-F, Körner C. 2011. Drought-sensitivity ranking of deciduous tree species based on thermal imaging of forest canopies. Agric For Meteorol. 151: 1632-1640.
Schwarz PA, Fahey TJ, Dawson TE. 1997. Seasonal air and soil temperature effects on photosynthesis in red spruce (*Picea rubens*) saplings. Tree Physiol. 17: 187-194.
Seidl R, Rammer W, Jäger D, Lexer MJ. 2008. Impact of bark beetle (*Ips typographus* L.) disturbance on timber production and carbon sequestration in different management strategies under climate change. For Ecol Manage. 256: 209-220.
Solberg S, Næsset E, Hanssen KH, Christiansen E. 2006. Mapping defoliation during a severe insect attack on Scots pine using airborne laser scanning. Remote Sens Environ. 102: 364-376.
Soliman A, Heck RJ, Brenning A, Brown R, Miller S. 2013. Remote sensing of soil moisture in vineyards using airborne and ground-based thermal inertia Data. Remote Sens. 5: 3729-3748.
Solomon S, Qin D, Manning M, Chen Z, Marquis M, Averyt K, Tignor M, Miller H. 2007. IPCC, 2007: climate change 2007: the physical science basis. Contribution of Working Group I to the fourth assessment report of the Intergovernmental Panel on Climate Change.
Townsend PA, Singh A, Foster JR, Rehberg NJ, Kingdon CC, Eshleman KN, Seagle SW. 2012. A general Landsat model to predict canopy defoliation in broadleaf deciduous forests. Remote Sens Environ. 119: 255-265.
Vastaranta M, Kantola T, Lyytikäinen-Saarenmaa P, Holopainen M, Kankare V, Wulder MA, Hyyppä J, Hyyppä H. 2013a. Area-based mapping of defoliation of scots pine stands using airborne scanning LiDAR. Remote Sens. 5: 1220-1234.
Vastaranta M, Korpela I, Uotila A, Hovi A, Holopainen M. 2012. Mapping of snow-damaged trees based on bitemporal airborne LiDAR data. Eur J For Res. 131: 1217-1228.
Vastaranta M, Wulder MA, White JC, Pekkarinen A, Tuominen S, Ginzler C, Kankare V, Holopainen M, Hyyppä J, Hyyppä H. 2013b. Airborne laser scanning and digital stereo imagery measures of forest structure: Comparative results and implications to forest mapping and inventory update. Can J Remote Sens. 39: 382-395.
Weber FP. 1971. The use of airborne spectrometers and multispectral scanners for previsual detection of Ponderosa pine trees under stress from insects and disease. Monitoring forest land from high altitude and from space. Office of Space Science and Application, NASA, Houston, Texas, 94-104.
Veltheim T. 1987. [Height models for pine, spruce and birch] [dissertation]. Helsinki (Finland): University of Helsinki. Finnish.
Wermelinger B. 2004. Ecology and management of the spruce bark beetle *Ips typographus* — a review of recent research. For Ecol Manage. 202: 67-82.

White JC, Wulder MA, Brooks D, Reich R, Wheate RD. 2005. Detection of red attack stage mountain pine beetle infestation with high spatial resolution satellite imagery. Remote Sens Environ. 96: 340-351.
Wulder MA, White J, Bentz B, Alvarez M, Coops N. 2006. Estimating the probability of mountain pine beetle red-attack damage. Remote Sens Environ. 101: 150-166.
Wulder MA, White JC, Coops NC, Butson CR. 2008. Multi-temporal analysis of high spatial resolution imagery for disturbance monitoring. Remote Sens Environ. 112: 2729-2740.
Vähäsaari H. 1988. [Evaluating timber assortment structure with different measuring methods] [dissertation]. Joensuu (Finland): University of Joensuu. Finnish.
Zarco-Tejada PJ, González-Dugo V, Berni JA. 2012. Fluorescence, temperature and narrow-band indices acquired from a UAV platform for water stress detection using a micro-hyperspectral imager and a thermal camera. Remote Sens Environ. 117: 322-337.

Table 1. The plot-wise (n = 53) averages and the variation of basal-area weighted mean diameter (*Dg*), Lorey's height (*Hg*), basal area (*G*), stem volume (*Vol*), age, percentage of defoliated stem volume (*Defol_V*) and percentage of dead stem volume (*Dead_V*) of the field data acquired in the fall of 2013.

Variable	Min	Max	Mean	StDev
Dg (cm)	12.6	40.3	24.3	6.4
Hg (m)	11.5	30.7	20.6	4.3
G (m^2/ha)	12.2	62.4	31.7	11.5
Vol (m^3/ha)	115.2	697.2	318.2	156.5
Age (years)	28.7	76.5	49.5	11.1
N (stems/ha)	275	3615	1175	710
Defol_V (%)	0	72.7	11.2	14.1
Dead_V (%)	0	94.0	12.9	19.4

Table 2. Statistics of the extracted thermal features for all plots.

Variable	Min	Max	Mean	StDev
$Plot_{mean}$	42.2	224.1	139.7	37.0
$Canopy\text{-}only_{mean}$	41.8	224.1	138.9	35.9
$Ground\text{-}only_{mean}$	50.9	224.2	137.5	38.3
$Plot_{min}$	0.0	196.0	98.9	40.4
$Canopy\text{-}only_{min}$	0.0	210.0	103.1	43.2
$Plot_{max}$	78.0	254.0	174.9	37.0
$Canopy\text{-}only_{max}$	78.0	243.0	171.2	33.7

Table 3. Statistics of the extracted light detection and ranging (LiDAR) features for all plots.

Feature	Description	Min	Max	Mean	StDev
CHM_mean (m)	Mean height of all first-echo points	0.42	21.04	9.52	4.98
CHM_max (m)	Maximum height of the laser points	3.45	34.33	20.83	6.94
CHM_std (m)	Standard deviation of the heights	0.68	10.59	6.12	2.23
CV	CHM_std divided by CHM_mean	0.31	2.78	0.80	0.38
ASL (m)	Mean height of the ground points above sea level	45.15	81.90	64.11	8.10
ASL_std (m)	Standard deviation of the ground points	0.06	1.79	0.63	0.41
Slope	The average degree of slope, calculated from DEM	1.66	20.50	8.48	4.55
Aspect	The direction of the slope, calculated from DEM	48.5	309.2	179.4	69.5
FCC (%)	Forest canopy cover percentage (over 3 meters from CHM)	1.18	94.90	66.03	22.61
H90 (m)	Heights of first-echo points at 90^{th} percentile	2.73	30.02	18.27	6.29
H80 (m)	Heights of first-echo points at 80^{th} percentile	2.32	29.10	17.05	6.13
H70 (m)	Heights of first-echo points at 70^{th} percentile	2.01	27.61	16.07	5.97
H60 (m)	Heights of first-echo points at 60^{th} percentile	1.73	26.91	15.20	5.83

Table 4. Stem volume classes for comparison of defoliated and healthy plots.

Name	Stem volume (m^3/ha)	n
Healthy 160	160–240	6
Defoliated 160	160–240	6
Healthy 240	240–320	4
Defoliated 240	240–320	5
Healthy 320	320–400	4
Defoliated 320	320–400	5
Healthy 400	> 400	4
Defoliated 400	> 400	5

Table 5. The coefficients of determination (R^2) and root-mean-squared-errors (RMSE) for the regression models with logarithmic transformation of stem volume (*log(Vol)*), defoliated stem volume (*Defol_V*) and standard deviation of canopy height model (*CHM_std*) as predictors, when mean surface temperature is predicted.

Predictors	R^2	RMSE
log(Vol)	0.16	33.62
log(Vol) + Defol_V	0.25	31.60
CHM_std	0.06	35.65
CHM_std + Defol_V	0.12	34.14

Table 6. The parameter estimates for intercept, logarithmic transformation of stem volume (*log(Vol)*) and defoliated stem volume when mean temperature is predicted using multiple regression analysis.

Predictor	Estimate	Std. error	*t* value	*p* value
Intercept	152.749	8.69	17.574	< 0.0001
log(Vol)	–16.304	3.654	−4.463	$3.63*10^{-5}$
Defoliated volume (%)	0.8907	0.317	2.809	0.0067

Table 7. The parameter estimates for intercept, CHM_std and defoliated stem volume when mean temperature is predicted using multiple regression analysis.

Predictor	Estimate	Std. error	*t* value	*p* value
Intercept	178.767	16.80	10.641	< 0.0001
CHM_std	−7.233	2.486	−2.910	0.0051
Defoliated volume (%)	0.8033	0.346	2.322	0.0236

Figure 1. a) Location of the study site. The background maps were provided by the National Land Survey of Finland. b) The thermal image mosaic with plot locations.

Figure 2. Relative mean surface temperature ($Plot_{mean}$) vs. forest structural variables in healthy plots (n = 43).

Figure 3. Relative mean surface temperature ($Plot_{mean}$) vs. LiDAR features in healthy plots (n = 43).

Figure 4. a) Defoliated plots vs. healthy plots in four stem volume classes. b) Relative mean temperature ($plot_{mean}$) in the healthy and the defoliated plots with 10–20% (*Defoliated 10%*) and over 20% (*Defoliated 20%*) of defoliated stem volume. N.B. Only plots with stem volumes over 100 m^3/ha were included.

Figure 5. a) Relative temperature difference between the canopy and the entire plot, plot-wise ($canopy\text{-}only_{mean} - plot_{mean}$), in the healthy and the defoliated plots with 10–20% (*Defoliated 10%*) and over 20% (*Defoliated 20%*) of defoliated stem volume. b) Standard deviation of the surface temperature recordings ($plot_{mean}$) in the healthy and the defoliated plots with 10–20% (*Defoliated 10%*) and over 20% (*Defoliated 20%*) of defoliated stem volume. N.B. Only plots with stem volumes over 100 m^3/ha were included.